

## **Comparative Evaluation of Convection Schemes for the Numerical Analysis of Thermal Stratification in a Horizontal Circular Pipe**

Yun Il Kim, Sang Jin Cho, Wee Kyung Kim, and Jong Chull Jo

Korea Institute of Nuclear Safety  
19 Kusung-dong, Yusung-ku, Taejon 305-338, Korea

### **Abstract**

This paper presents a comparative evaluation of four convection schemes, QUICK, HPLA, HYBRID and COPLA for the numerical analysis of unsteady stratified flow and conjugate heat transfer in a circular pipe. All the schemes are formulated on a non-uniform, non-orthogonal grid so that they can be applicable to the practical engineering flow calculations. The relative performances among the four schemes are investigated by applying them to the numerical analysis of thermal stratification in a pressurizer surge line of pressurized water reactor(PWR) plant. It is seen from the calculation results that all the bounded schemes might be applicable for the solutions of thermal stratification problem in a horizontal circular pipe, the HPLA and COPLA schemes results in nearly the same solution and are more superior both in accuracy and convergence to the QUICK and HYBRID schemes.

### **1. Introduction**

Development of an efficient convection scheme which is simple to implement but is free of false diffusion has been one of the major tasks for the computational fluid dynamicists over the last two decades. The classical lower-order schemes such as the upwind scheme, the hybrid central/upwind scheme and the power-law scheme[1] are unconditionally bounded and highly stable but highly diffusive when the flow direction is skewed relative to the grid lines. A simple remedy to overcome the false diffusion is to use a fine enough grid. However, such a practice is not practical due to the requirement of excessive computer storage and computational efforts, especially in the complex three-dimensional flow calculations.

Considerable efforts have been made toward the development of the improved differencing schemes, mainly in two directions. One is raising the order of the scheme and the other is taking into account the multidimensional nature of flow. The QUICK(Quadratic Upstream Interpolation for Convective Kinematics) scheme[2] and the second-order upwind scheme[3] belong to the former approach and the skew-upwind scheme[4] the latter. These schemes have been successful in increasing the accuracy of the solution, but all suffer from the boundedness problem, resulting in an oscillatory solution behavior in regions of steep gradient which can lead to the numerical instability.

Recently Gaskell and Lau[5] developed a higher-order bounded scheme named SMART(Sharp and Monotonic Algorithm for Realistic Transport) employing a composite approach in which the high resolution schemes are combined with the lower-order bounded schemes. Leonard[6] also proposed a similar bounded scheme of third-order accuracy named SHARP(Simple High-Accuracy Resolution Program). These two schemes have resolved the forementioned boundedness problem without much deteriorating the accuracy of the higher-order scheme. However, numerical experiments[7] have shown that these schemes need an under-relaxation treatment at each of the control volume cell faces in order to overcome the oscillatory convergence behaviors. This deficiency leads to the increase of the computer storage requirement, which may pose a practical constraint to their use in the complex three-dimensional turbulent flow calculations.

Subsequent studies by Zhu and Rodi[8], Zhu[9], Shin and Choi[10] and Choi et al[11] have proposed bounded convection schemes which are free of oscillatory convergence behaviors by choosing simple characteristics in the normalized variable diagram, such as piecewise-linear profile (SOUCUP : Second-Order

Upwind-Central differencing-first-order UPwind), a parabolic profile(HLPA: Hybrid Linear/Parabolic Approximation), a cubic profile (SMARTER: SMART Efficiently Revised) and a combination of piecewise linear profiles (COPLA: Combination Piecewise Liner Approximation). These schemes are very simple to implement and computationally cost effective. Recently, Choi and Lee[12] have evaluated some Higher-order bounded convection schemes the numerical solutions of the pure convection of a scalar variable problem and the laminar low in lid-driven cavity.

This study aims to perform the comparative evaluation of above four convection schemes, QUICK, HPLA HYBRID and COPLA, in the thermally stratified flow calculations under highly convective conditions. All the schemes are formulated on a non-uniform, non-orthogonal grid so that they can be applicable to the practical engineering flow calculations. The relative performances among the schemes are investigated by applying them to the numerical analyses of thermal stratification in a pressurizer surge line of pressurized water reactor(PWR) plant.

## 2. Mathematical Formulation

### 2.1 Governing Equations

To evaluate the applicability of four convection schemes considered herein to the numerical analysis of thermally stratified flow in a horizontal circular pipe, the thermal stratification in a pressurizer surge line of PWR plant [13-15] is chosen as a test problem in this study.

For this purpose, consider the same situation as in the work by Jo et al[14], where hot fluid and cold fluid flow in the PWR pressurizer surge line with a constant bulk velocity. The hot fluid occupies upper portion of the pipe (see Fig. 1). Consequently this leads to the formation of two distinct fluid layers in the pipe. For simplicity, it is assumed in this study that the flow is fully developed and the axial gradients of velocities and temperature are negligible. Thus the dimensionless governing equation of this thermally stratified flow model can be expressed in a generalized coordinate system  $x^j$  as [14],

$$\frac{\partial}{\partial x^1} U_1 + \frac{\partial}{\partial x^2} U_2 = 0 \quad (1)$$

$$\begin{aligned} & \frac{\partial}{\partial t} (Ju_1) + \frac{\partial}{\partial x^1} \left[ U_1 u_1 - \frac{1}{\text{Re} J} \left\{ \frac{\partial u_1}{\partial x^1} D_1^1 + \frac{\partial u_1}{\partial x^2} D_2^1 + b_1^1 w_1^1 + b_2^1 w_1^2 \right\} + P b_1^1 \right] \\ & + \frac{\partial}{\partial x^2} \left[ U_2 u_1 - \frac{1}{\text{Re} J} \left\{ \frac{\partial u_1}{\partial x^1} D_1^2 + \frac{\partial u_1}{\partial x^2} D_2^2 + b_1^2 w_1^1 + b_2^2 w_1^2 \right\} + P b_1^2 \right] = \frac{Gr}{\text{Re}^2} T J \end{aligned} \quad (2)$$

$$\begin{aligned} & \frac{\partial}{\partial t} (Ju_2) + \frac{\partial}{\partial x^1} \left[ U_1 u_2 - \frac{1}{\text{Re} J} \left\{ \frac{\partial u_2}{\partial x^1} D_1^1 + \frac{\partial u_2}{\partial x^2} D_2^1 + b_1^1 w_2^1 + b_2^1 w_2^2 \right\} + P b_2^1 \right] \\ & + \frac{\partial}{\partial x^2} \left[ U_2 u_2 - \frac{1}{\text{Re} J} \left\{ \frac{\partial u_2}{\partial x^1} D_1^2 + \frac{\partial u_2}{\partial x^2} D_2^2 + b_1^2 w_2^1 + b_2^2 w_2^2 \right\} + P b_2^2 \right] = 0 \end{aligned} \quad (3)$$

$$\frac{\partial}{\partial t} (JT) + \frac{\partial}{\partial x^1} \left[ U_1 T - \frac{1}{\text{Re} Pr J} \left\{ \frac{\partial T}{\partial x^1} D_1^1 + \frac{\partial T}{\partial x^2} D_2^1 \right\} \right] + \frac{\partial}{\partial x^2} \left[ U_2 T - \frac{1}{\text{Re} Pr J} \left\{ \frac{\partial T}{\partial x^1} D_1^2 + \frac{\partial T}{\partial x^2} D_2^2 \right\} \right] = 0 \quad (4)$$

where

$$\begin{aligned} U_1 &= (u_1 b_1^1 + u_2 b_2^1), \quad U_2 = (u_1 b_1^2 + u_2 b_2^2), \quad D_m^j = b_k^j b_k^m, \quad w_j^i = \frac{\partial u_i}{\partial x^k} b_j^k \\ \text{Re} &= \frac{W_0 r_i}{\boldsymbol{n}}, \quad \text{Pr} = \frac{c_p \boldsymbol{m}}{k}, \quad Gr = \frac{g \boldsymbol{b} r_i^3 (T_h - T_c)}{\boldsymbol{n}^2} \end{aligned} \quad (5)$$

and the geometric coefficients  $b_i^j$  represent the cofactors of  $\partial y^i / \partial x^j$  in the Jacobian matrix of the coordinate transformation  $y^i = y^i(x^j)$ , and  $J$  is the determinant of the Jacobian matrix. In the above equations (1) - (4),  $\boldsymbol{r}$ ,  $\boldsymbol{m}$ ,  $p$ ,  $k$ ,  $c_p$ ,  $\boldsymbol{b}$ , and  $g$  denote respectively density, dynamic viscosity, pressure, thermal conductivity, the specific heat, volumetric coefficient of thermal expansion, and the gravitational acceleration. In addition,  $u_i$  are the Cartesian velocity components in the  $y^i$  direction,  $W_0$  is a specified constant bulk velocity of

stratified fluid in the  $x^3$  direction, and  $r_i$  is the inner radius of the pipe.

## 2.2 Initial and Boundary Conditions

As mentioned previously, the pipe wall is initially at the temperature of cold fluid  $T_c$ , and is suddenly exposed to hot fluid at  $T_h$ . The initial conditions for this are given as

$$u_i = 0 \quad (i = 1, 2) \quad \text{in the whole solution domain, } t = 0 \quad (6a)$$

$$T = 0 \quad \text{in the pipe wall and the cold fluid layer, } t = 0 \quad (6b)$$

$$T = 1 \quad \text{in the hot fluid layer, } t = 0 \quad (6c)$$

Because the solution domain is symmetrical thermally and geometrically, only half of the region is needed to analyze. Thus along the symmetry line, the symmetry boundary conditions is applied for both velocity and temperature. On the solid wall, the velocity of the fluids vanishes. For this situation the boundary conditions are given by

$$u_i = 0 \quad (i = 1, 2) \quad \text{at the inner surface of the pipe, } t > 0 \quad (7a)$$

$$\frac{\partial T}{\partial n} = -\frac{B_i(T - T_\infty)}{a} \quad \text{at the outer surface of the pipe, } t > 0 \quad (7b)$$

$$\text{where } a = (r_o - r_i)/r_i \quad \text{and} \quad B_i = h(r_o - r_i)/k_s$$

$$u_2 = 0, \quad \frac{\partial u_1}{\partial x^1} = 0, \quad \frac{\partial T}{\partial x^1} = 0 \quad \text{at the symmetry plane, } t > 0 \quad (7c)$$

where  $n$  is the outward normal to the surface of the wall,  $T_\infty$  is the temperature of environment outside the pipe,  $h$  is heat transfer coefficient,  $k_s$  is the thermal conductivity of the pipe material, and  $r_o$  is the outer radius of the pipe.

## 2.3 Solution Domain Discretization

The governing equations (1) – (4) are solved numerically by a finite volume approach, requiring the discretization of the solution domain into a finite number of quadrilateral control volume cell whose faces are coincided with the non-orthogonal curvilinear coordinate lines.

A typical discretized domain is presented in Fig. 2, and also a typical control volume cell is shown in Fig. 3. The values of all computed variables are stored at the geometric center of each control volume cell. The interface between the hot and cold fluids is arranged here to align with a boundary between two rows of cells, i.e. a gridline.

To obtain the curvilinear non-orthogonal mesh shown in Fig. 2, it is assumed that the solution domain is the cross-section of a pair of eccentric cylinders as shown in Fig. 4. The center of the inner solid cylinder is coincided with the intersecting point of the fluid interface and the vertical symmetry line passing the center of the pipe.

The outer cylinder is the pipe subjected to internally stratified flow, and the inner cylinder has such a small size of diameter that the effect of its presence on the calculations can be negligible. Thus, the following boundary conditions are applied to the outer surface of the inner solid cylinder with such an infinitesimal diameter.

$$\frac{\partial u_i}{\partial x^2} = 0, \quad \frac{\partial T}{\partial x^2} = 0 \quad (i = 1, 2) \quad \text{at the outer surface of the infinitesimal inner cylinder, } t > 0 \quad (8)$$

Dislocating the inner solid cylinder either downward or upward can easily control the level of the fluid interface with a horizontal straight-line configuration. The grid is generated by using an algebraic method. In this study, the calculations are performed with a grid of 77×62, forming 76 divisions in the circumferential direction and 61 divisions in the radial direction.

## 2.4 Momentum Interpolation Method

For a better resolution of flow field in complex geometries, recently several investigators have developed various calculation methods of momentum equations employing the non-orthogonal, body-fitted coordinates. Among these methods, the non-staggered, momentum interpolation method originally developed by Rhie and

Chow [16] is known to be one of the efficient methods and has been widely used because of its simplicity feature of algorithm. In this method, the momentum equations are solved at the cell centered locations using the Cartesian velocity components as dependent variables and the cell face velocities are obtained through the interpolation of the momentum equations for the neighboring cell centered Cartesian velocity components. In the present analysis, the modified version of the Rhie and Chow's scheme [15] is used to obtain a converged solution of unsteady flow that is independent of the size of time step.

## 2.5 Discretization of Transport Equations

In the finite volume approach, the transport equations, Eqs. (1)- (4), are integrated over a control volume shown in Fig. 3. The resulting equation of a general dependent variable  $f$  can be written as follows

$$(a_p - a_{p-1}) \frac{DV}{Dt} + F_e - F_w + F_n - F_s = S_f DV + S_f^b \quad (9)$$

where  $a_p$  and  $a_{p-1}$  denote, respectively, the new and previous values of variable at the nodal point  $p$ .  $\Delta V$  and  $\Delta t$  mean the control volume and the time step, respectively.  $F$  represents the total flux of  $f$  across the cell face and  $S_f^b$  is the sum of the non-orthogonal diffusion terms. The total flux at the west face, for example, can be written as follows with the diffusion term approximated by the central differencing scheme.

$$F_w = C_w f_w - D_w (f_p - f_w) \quad (10)$$

where

$$C_w = (rU)_w, \quad D_w = \left( \frac{\Gamma_f}{J} D_1^1 \right) \quad (11)$$

The evaluation of  $f_w$  plays a key role in determining the accuracy and the stability of numerical solutions. For example, the  $f_w$  is evaluated as follows when one uses the first-order upwind scheme

$$f_w = U_w^+ f_w + U_w^- f_p \quad (12)$$

where  $U_w^+$  and  $U_w^-$  are the indicators of the local velocity direction such that

$$\begin{aligned} U_w^+ &= 0.5(1 + |U_w|/U_w), \\ U_w^- &= 1 - U_w^+ \quad (U_w \neq 0) \end{aligned} \quad (13)$$

Incorporation of Eq. (10) and Eq. (12) and similar expressions for the other cell faces leads to following general difference equation

$$A_p f_p = A_E f_E + A_W f_W + A_N f_N + A_S f_S + b_f \quad (14)$$

where

$$\begin{aligned} A_W &= D_w + C_w U_w^+ \\ A_E &= D_e - C_e U_e^- \\ A_S &= D_s + C_s V_s^+ \\ A_N &= D_n - C_n V_n^- \\ A_p &= A_E + A_W + A_N + A_S - S_f^P \Delta V \\ b_f &= S_f^C \Delta V + S_f^b \end{aligned} \quad (15)$$

and  $S_f^C, S_f^P$  are the linearized source terms.

The details of implementation of the higher-order bounded schemes will be outlined in the following chapter.

### 3. Higher-Order Bounded Schemes [12]

The current high-order bounded schemes are based on the variable normalization by Leonard[6] and the convection boundedness criterion by Gaskell and Lau[5]. Consider, without loss of generality, the west face of control volume. We introduce a normalized variable such that

$$\hat{f} = \frac{f - f_U}{f_D - f_U} \quad (16)$$

where the subscripts U and D denote the upstream and the downstream locations. Eq. (16) can be rewritten in terms of nodal point values

$$\hat{f} = \frac{f - f_{WW}}{f_D - f_{WW}} U_w^+ + \frac{f - f_E}{f_W - f_E} U_w^- \quad (17)$$

Using the above upwind biased normalized variable, the following four schemes can be written as follows:

#### Central difference scheme

$$\hat{f}_w = [(1 - C_2)\hat{f}_W + C_2]U_w^+ + [C_2\hat{f}_P + (1 - C_2)]U_w^- \quad (18)$$

#### First-order upwind scheme

$$\hat{f}_w = \hat{f}_W U_w^+ + \hat{f}_P U_w^- \quad (19)$$

#### Second-order upwind scheme

$$\hat{f}_w = (1 - C_1)\hat{f}_W U_w^+ + (1 - C_3)\hat{f}_P U_w^- \quad (20)$$

#### QUICK scheme

$$\hat{f}_w = \left[ (1 + C_1)(1 - C_2)\hat{f}_W + C_2 \left( 1 - \frac{C_1(1 - C_2)}{C_1 + C_2} \right) \right] U_w^+ + \left[ C_2(1 + C_3)\hat{f}_P + (1 - C_2) \left( 1 - \frac{C_2 C_3}{1 - C_2 + C_3} \right) \right] U_w^- \quad (21)$$

where

$$C_1 = \frac{\Delta X_W}{\Delta X_W + \Delta X_{WW}}, \quad C_2 = \frac{\Delta X_W}{\Delta X_W + \Delta X_P}, \quad C_3 = \frac{\Delta X_W}{\Delta X_P + \Delta X_E} \quad (22)$$

are the geometric interpolation factors defined in terms of the size of control volume cell. For example, is the size of control volume around the calculation point P and is defined as

$$\Delta X_P = \overline{wP} + \overline{Pe} \quad (23)$$

The normalized diagrams for these well-known schemes ( $U_w > 0$ ) are shown in Fig. 5.

Gaskell and Lau[5] formulated following convection boundedness criterion. Define a continuous increasing function or union of piecewise continuous increasing function F relating the modeled normalized face value  $\hat{f}_w$  to the normalized upstream nodal value  $\hat{f}_W (U_w > 0)$ , that is  $\hat{f}_w = F(\hat{f}_W)$ . Then a finite difference approximation to  $\hat{f}_w$  is bounded if

- (i) for  $0 \leq \hat{f}_W \leq 1$ , F is bounded below by the function  $\hat{f}_w = \hat{f}_W$  and above by unity and passes through the points (0,0) and (1,1);
- (ii) for  $\hat{f}_W < 0$ ,  $\hat{f}_W > 1$ , F is equal to  $\hat{f}_w$ .

The convection boundedness criterion is a necessary and sufficient condition for achieving computed boundedness if only three neighboring upstream nodal values are used to approximate representation of the

convection boundedness criterion is shown in Fig. 6.

According to Leonard[6], for any(in general non-linear) characteristics in the normalized variable diagram(Fig. 5),

- (i) passing through Q is necessary and sufficient for second-order accuracy
- (ii) passing through Q with a slope of 0.75(for a uniform grid) is necessary and sufficient for third-order accuracy.

The horizontal and vertical coordinates of point Q in the normalized variable diagram and the slope of the characteristics at the point Q for preserving the third order accuracy for a non-uniform grid can be obtained by a simple algebra using Eqs. (18)-(21).

$$\begin{aligned}
 X_Q &= \frac{C_2}{C_1 + C_2} U_w^+ + \frac{1 - C_2}{1 - C_2 + C_3} U_w^- \\
 Y_Q &= \frac{C_2(1 + C_1)}{C_1 + C_2} U_w^+ + \frac{(1 - C_2)(1 + C_3)}{1 - C_2 + C_3} U_w^- \\
 S_Q &= (1 + C_1)(1 - C_2) U_w^+ + C_2(1 + C_3) U_w^-
 \end{aligned} \tag{24}$$

For a uniform grid,  $X_Q=0.5$ ,  $Y_Q=0.75$  and  $S_Q=0.75$  Following the above criteria by Gaskell and Lau[5] and by Leonard[6], one may choose several bounded characteristics in the normalized variable diagram whose order of accuracy is determined by the shape of the characteristics. Following are four simple possibilities which ensure the second or third-order accuracy.

#### The HPLA scheme

In this scheme, the normalized face value is approximated by a combination of linear and parabolic characteristics passing through the point, O, Q and P in the normalized variable diagram

$$\begin{aligned}
 \hat{f}_w &= a_w + b_w \hat{f}_C + c_w \hat{f}_C^2 \quad 0 \leq \hat{f}_C \leq 1 \\
 &= \hat{f}_C \quad \text{otherwise}
 \end{aligned} \tag{25}$$

where

$$\begin{aligned}
 a_w &= 0 \\
 b_w &= (Y_Q - X_Q^2) / (X_Q - X_Q^2) \\
 c_w &= (X_Q - Y_Q) / (X_Q - X_Q^2)
 \end{aligned} \tag{26}$$

Zhu[9] developed this scheme on the assumption of uniform grid( in this case),  $a_w=0, b_w=0, c_w=-1$ . The original scheme is further extended for use on the non-uniform grid in the present study. This scheme is second-order accurate.

#### The COPLA scheme

Another possible way of devising a third-order accurate scheme is to employ a composite of piecewise linear characteristics in which the QUICK scheme is employed in a range of  $0.5X_Q \leq \hat{f}_C \leq 1.5X_Q$ . This scheme is similar to the SMART scheme[5], but is free of convergence oscillation. Such a scheme was proposed by Choi et al[11] employing following characteristics in the normalized variable

$$\begin{aligned}
 \hat{f}_w &= a_w + b_w \hat{f}_C \quad 0 \leq \hat{f}_C \leq 0.5X_Q \\
 &= c_w + d_w \hat{f}_C \quad 0.5X_Q \leq \hat{f}_C \leq 1.5X_Q \\
 &= e_w + f_w \hat{f}_C \quad 1.5X_Q \leq \hat{f}_C \leq 1 \\
 &= \hat{f}_C \quad \text{otherwise}
 \end{aligned} \tag{27}$$

where

$$\begin{aligned}
a_w &= 0 \\
b_w &= (2Y_Q - S_Q X_Q) / X_Q \\
c_w &= Y_Q - S_Q X_Q \\
d_w &= S_Q \\
e_w &= (3X_Q - 2Y_Q - S_Q X_Q) / (3X_Q - 2) \\
f_w &= (2Y_Q + S_Q X_Q - 2) / (3X_Q - 2)
\end{aligned} \tag{28}$$

The normalized variable diagrams for the higher-order bounded schemes considered in the present study are given in Fig. 7.

It is worthwhile mentioning here that the present bounded schemes are very similar to the shock capturing schemes based on the Total Variational Diminishing flux limiters(TVD), which are widely used in the compressible flow calculations. The SOUCUP scheme is similar to the MINMOD(MINimum MODulus) scheme of Roe[17] and the HLP scheme is similar to the CLAM(Curved Line Advection Method) scheme of Van Leer[18]. The implementation of the higher-order bounded schemes is quite simple. We note that the forementioned four bounded schemes employ very similar forms of characteristics in the normalized variable diagram. They differ only in the order of the characteristics and the values of the constants. Therefore, it suffices to present the implementation of one scheme here, for example, the HLP scheme. In the present work, the higher-order schemes are implemented in a deferred correction way proposed by Khosla and Rubin[19].

Eq. (25) can be expressed in terms of the unnormalized variable

$$\begin{aligned}
\mathbf{f}_w &= \left\{ \mathbf{f}_W + (\mathbf{f}_P - \mathbf{f}_{WW}) \left[ a_w^+ + (b_w^+ - 1) \left( \frac{\mathbf{f}_W - \mathbf{f}_{WW}}{\mathbf{f}_P - \mathbf{f}_{WW}} \right) + c_w^+ \left( \frac{\mathbf{f}_W - \mathbf{f}_{WW}}{\mathbf{f}_P - \mathbf{f}_{WW}} \right)^2 \right] \right\} U_w^+ \\
&+ \left\{ \mathbf{f}_P + (\mathbf{f}_W - \mathbf{f}_E) \left[ a_w^- + (b_w^- - 1) \left( \frac{\mathbf{f}_P - \mathbf{f}_E}{\mathbf{f}_W - \mathbf{f}_E} \right) + c_w^- \left( \frac{\mathbf{f}_P - \mathbf{f}_E}{\mathbf{f}_W - \mathbf{f}_E} \right)^2 \right] \right\} U_w^-
\end{aligned} \tag{29}$$

Given the switch factors

$$\begin{aligned}
\text{for } U_w > 0: a_w^+ &= 1 \text{ if } |\mathbf{f}_P - 2\mathbf{f}_W + \mathbf{f}_{WW}| < |\mathbf{f}_W - \mathbf{f}_E| \\
a_w^+ &= 0 \text{ otherwise}
\end{aligned} \tag{30}$$

$$\begin{aligned}
\text{for } U_w < 0: a_w^- &= 1 \text{ if } |\mathbf{f}_W - 2\mathbf{f}_P + \mathbf{f}_E| < |\mathbf{f}_W - \mathbf{f}_E| \\
a_w^- &= 0 \text{ otherwise}
\end{aligned} \tag{31}$$

the unnormalized form of Eq. (29) can be rewritten as

$$\mathbf{f}_w = U_w^+ \mathbf{f}_W + U_w^- \mathbf{f}_P + \Delta \mathbf{f}_w \tag{32}$$

where

$$\begin{aligned}
\Delta \mathbf{f}_w &= U_w^+ a_w^+ (\mathbf{f}_P - \mathbf{f}_{WW}) \left[ a_w^+ + (b_w^+ - 1) \left( \frac{\mathbf{f}_W - \mathbf{f}_{WW}}{\mathbf{f}_P - \mathbf{f}_{WW}} \right) + c_w^+ \left( \frac{\mathbf{f}_W - \mathbf{f}_{WW}}{\mathbf{f}_P - \mathbf{f}_{WW}} \right)^2 \right] \\
&+ U_w^- a_w^- (\mathbf{f}_W - \mathbf{f}_E) \left[ a_w^- + (b_w^- - 1) \left( \frac{\mathbf{f}_P - \mathbf{f}_E}{\mathbf{f}_W - \mathbf{f}_E} \right) + c_w^- \left( \frac{\mathbf{f}_P - \mathbf{f}_E}{\mathbf{f}_W - \mathbf{f}_E} \right)^2 \right]
\end{aligned} \tag{33}$$

After the evaluation of the additional term, the implementation of this scheme is the same as that of the first-order upwind scheme. In the SOUCUP and LPPA schemes, the constants are switched according to the value of  $\hat{f}_c$  at the same cell face and for the same flow direction.

#### 4. Application to the Test Problem

All the higher-order bounded schemes described in the previous chapter are implemented in a computer code designed to solve the unsteady conjugate heat transfer and stratified flow in a horizontal curved pipe. The

computer code uses a non-staggered grid arrangement and the SIMPLE[1] algorithm for pressure-velocity coupling.

The geometry of the surge line and the computational parameters used here are the same as those in references [14]. In operating reactors, the outer surface of the surge line is insulated with a little heat loss. The overall heat transfer coefficient of  $h=0.79 \text{ W/m}^2\text{C}$  was used in the present analysis. The surge flow rate of hot fluid in the line coming from the pressurizer was considered to be  $1.26 \times 10^{-2} \text{ m}^3/\text{sec}$ . The interface levels for this test problem is at height of  $0.5 d_i$  from the horizontal reference line passing through the bottom point of inner wall surface, where  $d_i$  is the inner diameter of the surge line. For simplifying the calculations, the fluids are assumed to be Newtonian with constant properties and the Boussinesq approximation is assumed to be valid. And on the basis of these assumptions the variables of length, time, velocity and temperature are non-dimensionalized, respectively, using the reference scales of  $r_i$ ,  $r_i/W_0$ ,  $W_0$ , and  $\Delta T = (T_h - T_c)$ .

The dimensionless time step used in the computations is 0.1. The iterative computation for each time step ceases when the maximum of the absolute sum of dimensionless residuals of momentum equations or energy equation, or pressure correction equation is less than  $10^{-6}$ . Relaxation factors of 0.7 and 1.0 were used for momentum equations and energy equation, respectively.

Fig. 8 displays the transient circumferential inner and outer wall temperature distributions by the four different convection schemes. The angles of 0 degree and 180 degree on the figure mean the top and bottom positions in the circumferential direction, respectively. Fig. 8 indicates for all the schemes that the wall temperatures increase as the non-dimensional time increase and as the angle decreases. It can be seen that the HYBRID scheme results in relatively more diffusive profiles than the other three convection schemes in the top and bottom positions, and the solution of the QUICK scheme trends to be higher than that of other schemes in the top position with slightly oscillatory solution. HLP and COPL schemes, however, results in nearly the same solution at the all non-dimensional time in the top and bottom positions on the inner and outer walls.

Fig. 9 presents the variations of the local Nusselt number as a function of the angle at six different elapsed times for the four convection schemes. The average Nusselt number decreases to zero with elapsing of time for all the schemes because the difference in temperature between the fluid and wall surface is decreased with increasing of the elapsed times as shown in Fig. 10. Also, the solutions of Nusselt number for the four convection schemes are nearly same, except that the QUICK scheme exhibits relatively high and oscillatory value in the top position at the early stage of thermal stratification, as shown in Fig. 9(d).

Fig. 10 displays the transient isotherms for the four convection schemes. In the early stage, the temperature gradient is very steep in the hot fluid region near the inner wall surface and the fluid interface, as can be expected. As time elapses, the temperature difference between the top and bottom positions of the pipe wall increases to a maximum value and then decreases to zero. As can be seen in the Fig. 10, all the schemes show nearly the same patterns, except that the HYBRID scheme displays slightly different transient isotherms. Although the HYBRID scheme takes a short time to reach at the steady-state condition, the scheme predicts the relatively low temperatures as shown in Fig. 10.

Fig. 11 shows the transient top to bottom wall temperature differences both at the inner and outer wall surfaces for the four convection schemes. As shown in Fig. 11, the maximum value of temperature difference is higher at the inner wall surface than that at the outer wall surface. For the three schemes except the HYBRID scheme, it increases to their maximum values at the non-dimensional time of 1800 and then decreases as the time elapses further. For the HYBRID scheme, the top to bottom temperature difference is calculated to reach its maximum value at the non-dimensional time, 1000. Fig. 11 also shows that the HLP and COPL schemes result in nearly the same solution and the maximum top to bottom temperature difference is dependent on the convection scheme.

## 5. Conclusion

To evaluate the applicability of four convection schemes, QUICK, HLP, HYBRID and COPL to the numerical analysis of thermal stratification problem in a horizontal circular pipe, in this study the thermal stratification in a pressurizer surge line of PWR plant is chosen as a test problem and the relative performances among the four schemes are investigated. The following important conclusions can be drawn from the present analysis.

- All the bounded schemes might be acceptable for the applications to the solutions of thermal stratification problem in a horizontal circular pipe.
- QUICK scheme exhibits relatively high and oscillatory value in the top position at the early stage

of thermal stratification.

- HYBRID scheme results in relatively more diffusive profiles than the other three convection schemes in the top and bottom positions.
- The HPLA and COPLA schemes results in nearly the same solution and are more superior both in accuracy and convergence to the QUICK and HYBRID schemes.

## References

1. Patankar, S.V., Numerical Heat Transfer and Fluid Flow (McGraw-Hill, New York, 1980).
2. Leonard, B.P., "A stable and accurate convective modeling procedure based on quadratic interpolation," Comput. Methods Appl. Mech. Eng. Vol. 19 (1979), pp.59-98.
3. Warming, R.F. and Beam, F.M., "Upwind second order differences schemes and applications in aerodynamic flows," AIAA J. Vol. 14 (1976), pp.1241-1249.
4. Raithby, G.D., "Skew upstream differencing schemes for problem involving fluid flow," Comput. Methods Appl. Mech. Eng. Vol. 9 (1979), pp.153-164.
5. Gaskell, P.H. and Lau, A.K.C., "Curvature-compensated convective transport: SMART, a new boundedness preserving transport algorithm," Int. J. Numerical Methods Fluids Vol. 8 (1988), pp.617-641.
6. Leonard, B.P., "Simple high-accuracy resolution program for convective modeling of discontinuities," Int. J. Numerical Methods Fluids Vol. 8 (1988), pp.1291-1318.
7. Zhu, J., "On the higher-order bounded discretization schemes for finite volume computations of incompressible flows," Comput. Methods Appl. Mech. Eng. Vol. 98 (1992), pp.345-360.
8. Zhu, J. and Rodi, W., "A low dispersion and bounded convection scheme," Comput. Methods Appl. Mech. Eng. Vol. 92 (1991), pp.225-232.
9. Zhu, J., "A low-diffusive and oscillation free convection scheme," Comm. Appl. Numerical Methods Vol. 7 (1991), pp.225-232.
10. Shin, J.K. and Choi, Y.D., "Study on the improvement of the convective differencing scheme for the high-accuracy and stable resolution of the numerical solution," Trans. KSME Vol. 16, No.6 (1992), pp.1179-1194.
11. Choi, S.K. and Nam, H.Y. and Cho, M., "Evaluation of a higher-order bounded convection scheme three dimensional numerical experiments," Numerical Heat Transfer, part B, Vol. 28 (1995), pp.23-38.
12. Choi, S.K. and Lee, Y.B., "An evaluation of recent higher-order bounded convection schemes," *Journal of Numerical Heat Transfer*, Vol. 2, No. 1 (1997).
13. Jo, J.C., Kim, Y.I., Min, B.K., Oh, K.M. and Choi, S.K., "Numerical analysis of thermally stratified flow in the pressurizer surge line," Proc. Of '98 KNS Autumn Meeting(1998).
14. Jo, J.C., Kim, Y.I. and Shin, W.K., "Heat transfer analysis of thermal stratification in pressurizer surge line," Proc. of SmiRT- 15(1999), Vol. II pp.61-68.
15. Jo, J.C., Kim, Y.I. and Choi, S.K., "Numerical analysis of thermally stratified flow in a circular pipe line," Symposium on Emerging Technologies for Fluids, Structures, and Fluid/Structure Interactions, Proc. of ASME PVP Conference(1999).
16. Rhie, C.M. and Chow W.L., "Numerical study of the turbulent flow past a airfoil with trailing edge separation," AIAA J. Vol. 21 (1983), pp.1525-1532.
17. Roe, P.L., "Characteristic-based schemes for the Euler equations," in M Van Dyke et al., eds., Annual Reviews of Fluid Mechanics, Vol. 18 (Annual Reviews CA, 1986) pp.337.
18. Van Leer, B., "Towards the ultimate conservative difference scheme II Monotonicity and conservation combined in a second order scheme," J. Compt. Phys. Vol. 14 (1974), pp. 361-370.
19. Khosla, P.K. and Rubin, S.G., "A diagonally dominant second order accurate implicit scheme," Comput. Fluids 2 (1974), pp.207-209.

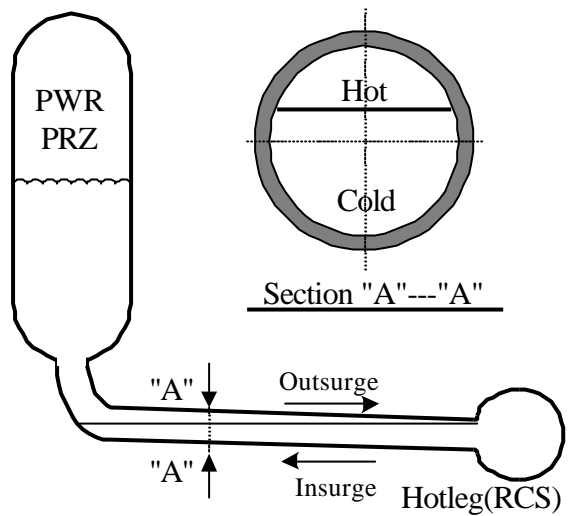


Fig. 1 Thermally stratified flow in a circular pipe.

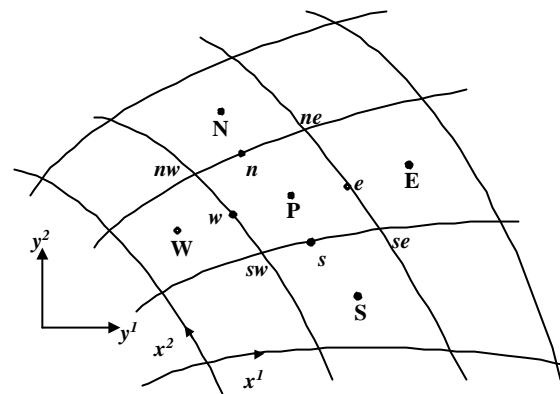


Fig. 3 A typical control volume cell in the computing mesh.

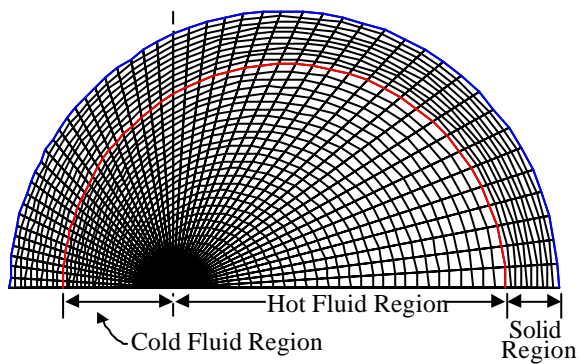


Fig. 2 The curvilinear non-orthogonal mesh.

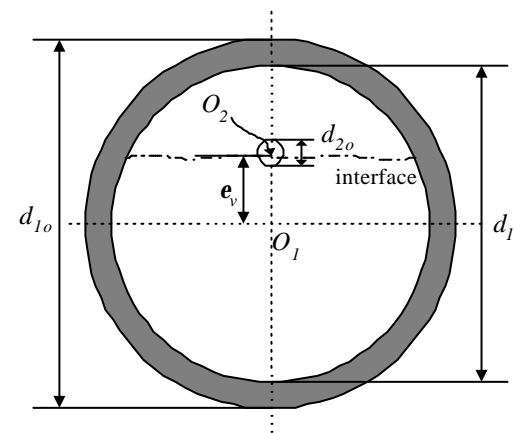


Fig. 4 The imaginary eccentric cylinder for mesh generation.

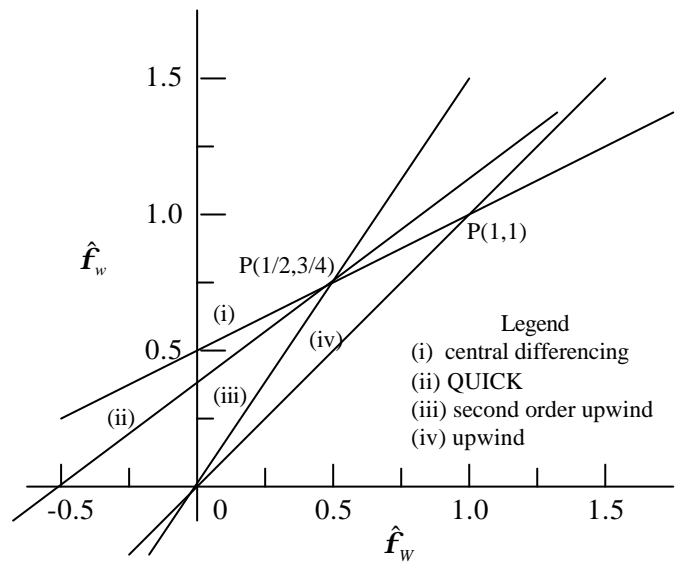


Fig. 5 The normalized variable diagram for various well-known schemes.

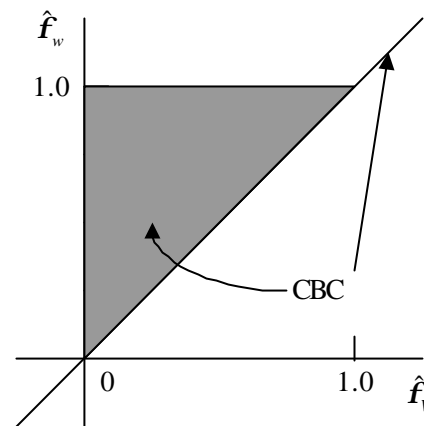


Fig. 6 Diagrammatic representation of the convection boundedness criterion.

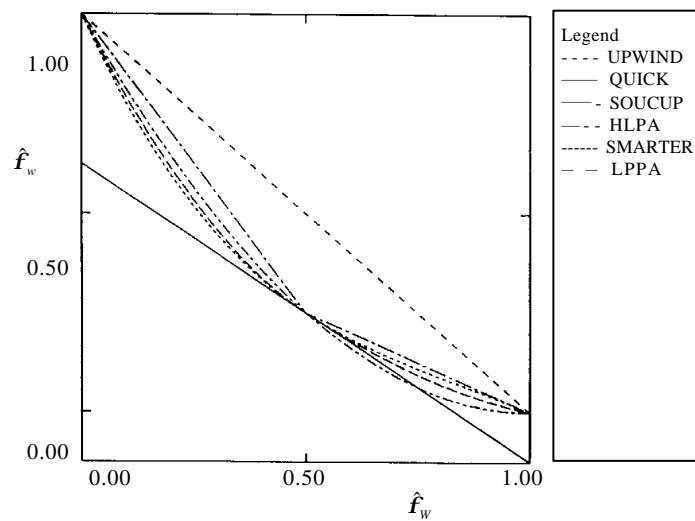
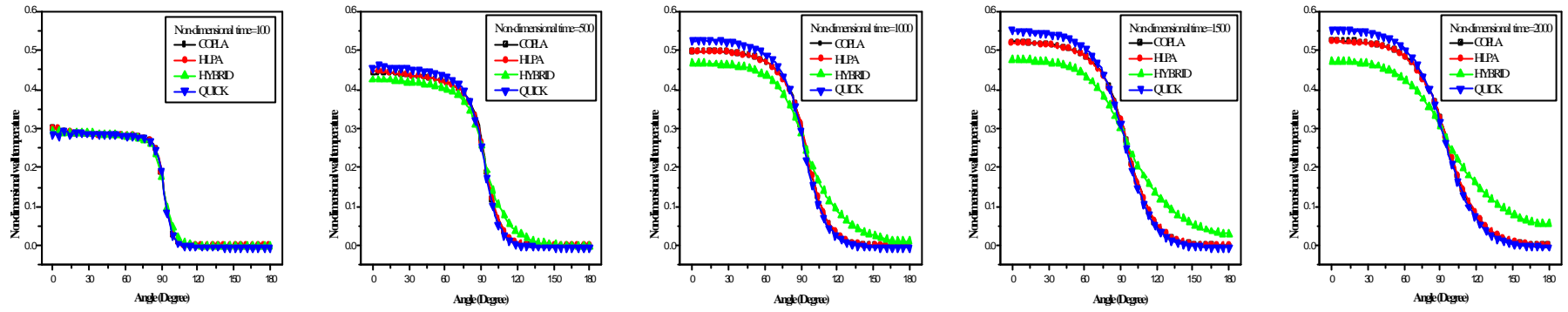
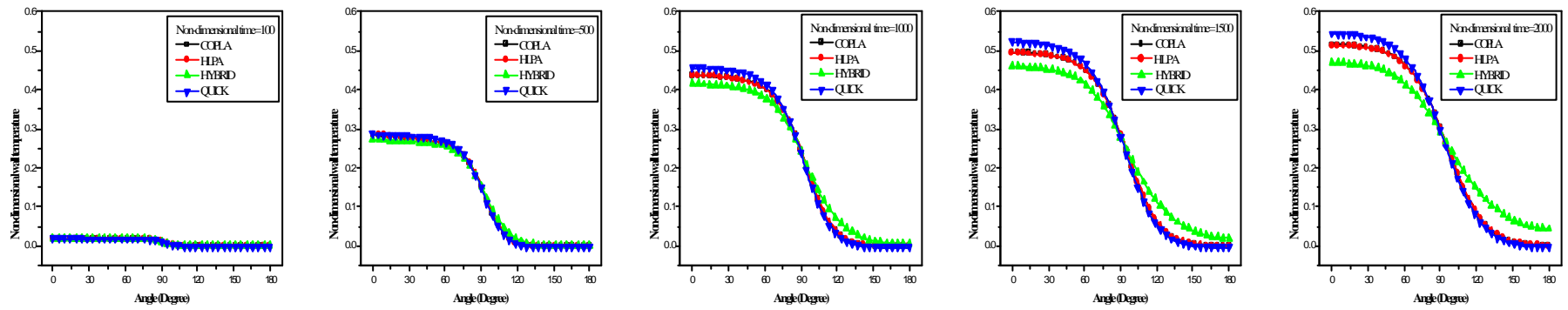


Fig. 7 The normalized variable diagram for bounded schemes.

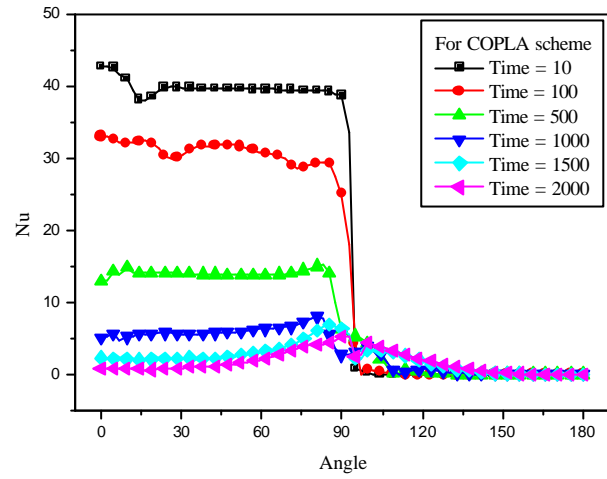


(a) on the inner wall

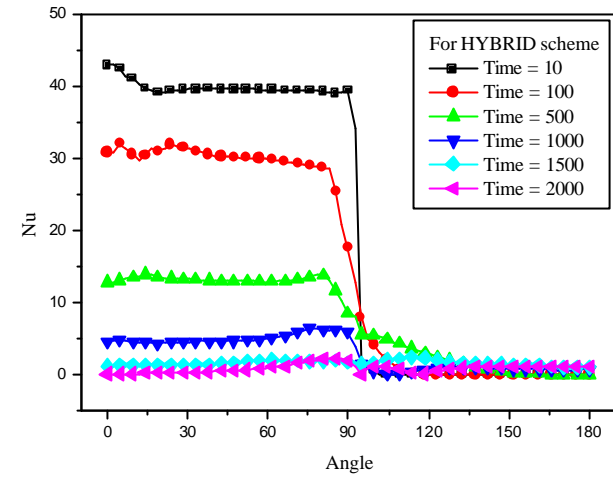


(b) on the outer wall

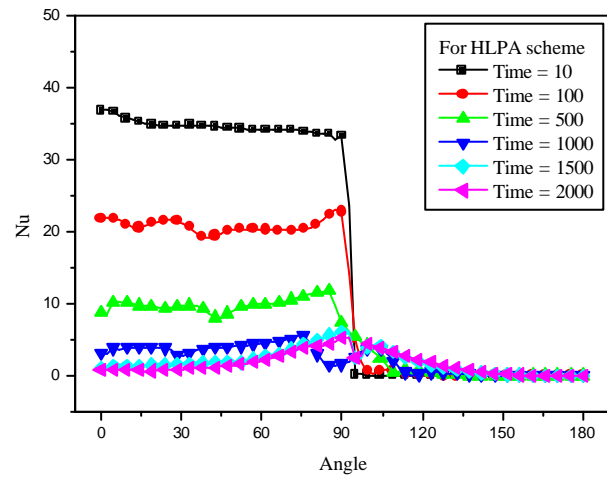
Fig. 8 Transient top to bottom wall temperature distributions.



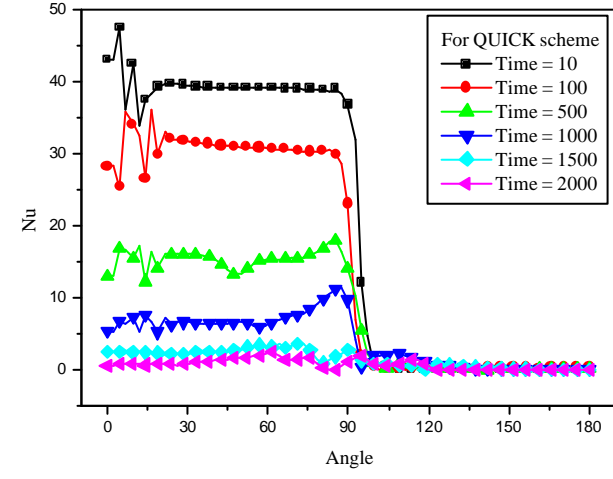
(a) COPLA scheme



(b) HPLA scheme

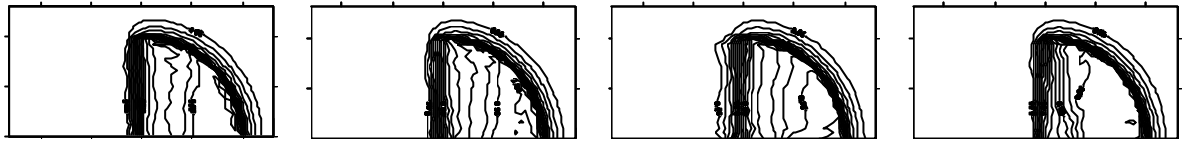


(c) HYBRID scheme

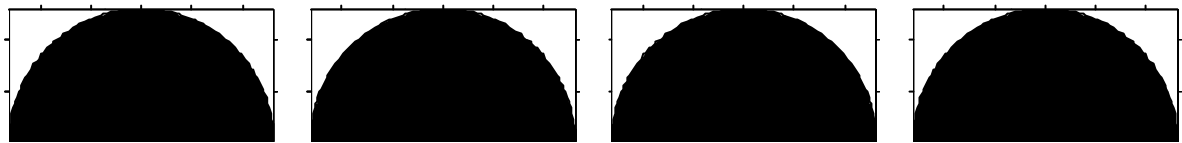


(d) QUICK scheme

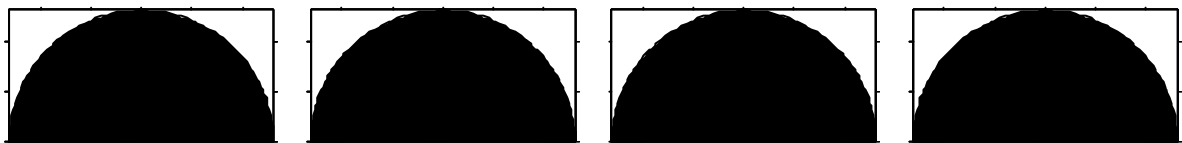
Fig. 9 The variation of the local Nusselt number(Nu).



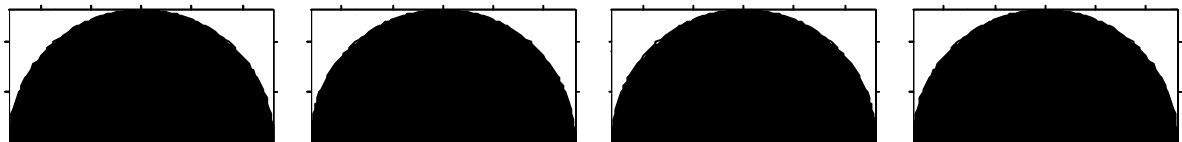
(a) Non-dimensional time = 100



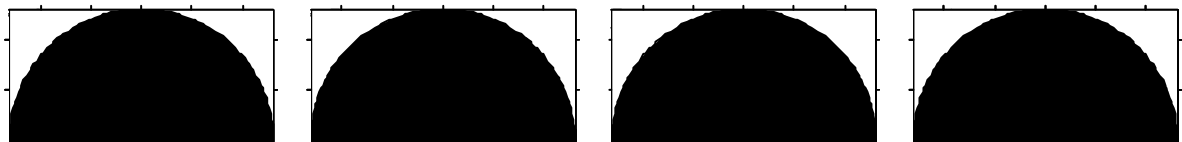
(b) Non-dimensional time = 500



(c) Non-dimensional time = 1000

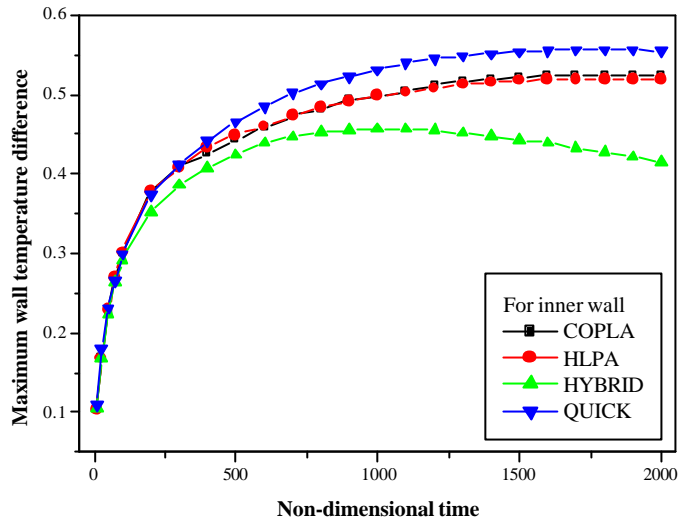


(d) Non-dimensional time = 1500

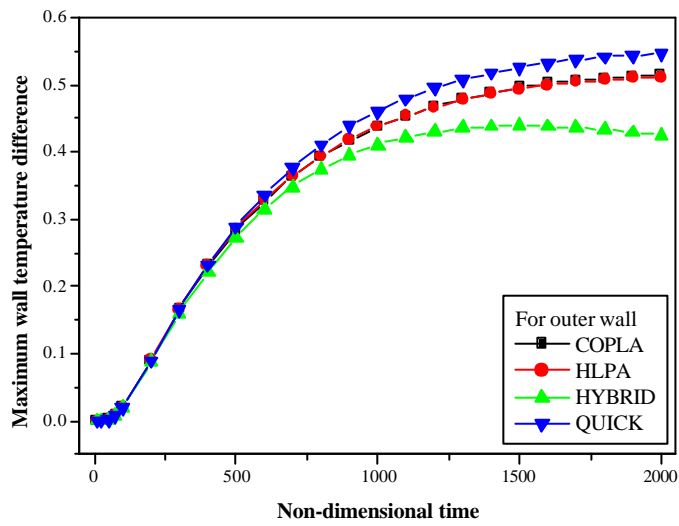


(e) Non-dimensional time = 2000

Fig. 10 Transient isotherms for the four convection schemes (COPLA, HLP, HYBRID, QUICK)



(a) For inner wall



(b) For outer wall

Fig. 11 Transient maximum wall temperature differences both on the inner and outer wall surfaces.